Electronic Supplementary Information for

Axial Ligand Promoted Phosphate Tolerance of Atomically Dispersed Fe Catalyst Towards Oxygen Reduction Reaction

Jing Liu,[1] Jie Wang,[1] Linjuan Zhang,[2] Chaohua Fan,[1] Xin Zhou,[3] Bingsen Zhang,[4] Xuejing Cui,[1]

Jianqiang Wang,[2,] Yi Cheng,[5,]* Shuhui Sun,[6] Luhua Jiang[1,]**

[1] Electrocatalysis & Nanomaterial Laboratory, College of Materials Science & Engineering, Qingdao University of Science & Technology, Qingdao, 266042, China

[2] Key Laboratory of Interfacial Physics and Technology, Shanghai Institute of Applied Physics, Chinese Academy of Sciences, Shanghai 201800, China

[3] College of Environment and Chemical Engineering, Dalian University, Dalian 116622, China

[4] Shenyang National Laboratory for Materials Science, Institute of Metal Research, Chinese Academy of Sciences, Shenyang 110016, China

[5] Department of Environmental Engineering, School of Metallurgy and Environment, Central South University, Changsha, 410083, China

[6] Institute National de la Recherche Scientifique (INRS), Centre Énergie Matériaux et Télécommunications, Varennes, Québec J3X 1P7, Canada

∗Corresponding authors:

Jianqiang Wang, E-mail: wangjianqiang@sinap.ac.cn

Yi Cheng, E-mail: yi.cheng@csu.edu.cn

Luhua Jiang, E-mail: luhuajiang@qust.edu.cn

Table of Contents

Physical characterization

The morphology and structure of the samples were characterized by a scanning electron microscope (SEM, FEI Quanta 650 FEG) and a high-resolution transmission electron spectroscope (HRTEM, FEI Themis 60-300). High angle annular dark-field scanning transmission electron microscopy (HAADF-STEM) was conducted on FEI Tecnai F20. Powered X-ray diffraction (XRD) was performed on a Rigaku minFlex II using Cu K radiation. Raman spectroscopy was obtained on LabRam HR Evolution. Nitrogen-sorption isotherms were measured at 77K with a Micromeritics ASAP 2020 analyzer. Pore distribution and the specific surface area were analyzed by the Density Functional Theory (DFT) method. Raman spectra were collected on LabRam HR Evolution. The surface valence state and composition of the sample were examined by X-ray photoelectron spectroscopy (XPS, ESCALABXi). All the spectra were calibrated with the carbon (C1s, 284.6 eV). Fe and Zn K-edge X-ray absorption spectroscopy (XAS) were conducted at beamline 14W1 of the Shanghai Synchrotron Radiation Facility (SSRF), China. Data were recorded using a Si (111) double crystal monochromator in fluorescence mode for Fe and transmission mode for Zn. All extended X-ray absorption fine structure (EXAFS) data were analyzed using the program Demeter.[1] For all samples, the EXAFS oscillations were extracted from the normalized XAS spectra by subtracting the atomic background using a cubic spline fit to k3-weighted data, where k is the photoelectron wave number. The $\chi(k)$ functions were then Fourier transformed into R-space. The Fourier-transform window was in the k range 1.8–10 Å for Fe and in the k range 3–13 Å for Zn. The content of Fe in the sample is determined by inductively coupled plasma-atomic emission spectrometry (ICP-MS) by PerkinElmer Optima 2100DV spectrometer.

MEA fabrication and testing of low-temperature PEMFC

The MEA for the low-temperature PEMFC with an active area of 4 cm^2 based on the Fe-N-C-1100 cathode was made as follows. In brief, the catalyst ink was created by ultrasonically combining Fe-N-C-1100 catalysts with a Nafion solution and isopropanol for 4 hours. The catalyst ink was sprayed onto the gas diffusion layer (GDL) until the Fe-N-C-1100 loading reached 3.5 mg cm^2. The anode catalyst layer was created by spraying 60 wt. % Pt/C-JM ink with Nafion solution and isopropanol onto another GDL. The Pt loading was kept constant at 0.1 mg cm^2. The MEA was created by sandwiching the membrane (Nafion 211) between two catalyst-coated GDL and hot pressing them together for 90s at 120 °C under 0.4 MPa. The single cell was operated at the temperature of 70°C. The anode and cathode were fed by fully humid H_2 and O_2 at 0.1 L min^{-1} and 0.2 L min^{-1}, respectively.

DFT Calculation

Spin-polarized density functional calculations have been performed by the Vienna ab initio simulation package (VASP)[2,3] with the projector augmented wave (PAW) pseudopotentials.[4] The Perdew-Burke-Ernzerhof (PBE) parameterization of the generalized gradient approximation (GGA) was adopted for the exchange correlation.[5] The energy cutoff employed for plane-wave expansion was set to 500 eV. The dimensions of the Fe-N_4-doped graphene sheet were calculated to be a=b=12.32 Å. The supercells were repeated periodically on the x-y plane while a vacuum region of 20 Å was applied along the z-direction to avoid mirror interaction between adjacent supercells. The Brillouin zone integration was sampled on a grid of 3×3×1 k-points for structural optimization and electronic structure calculation. All atoms were relaxed until the Hellman-Feynman forces on individual atoms were less than 0.01 eV/Å. To describe the static electronic correlation effect in the Fe 3d states, we applied the Hubbard U correction in the rotationally

invariant formalism.[6] We used U_{eff} (=*U*-*J*) of 4.3 eV on the Fe 3d states according to the literature.[7] Van der Waals correction has been considered by utilizing the DFT-D2 approach of Grimme.[8,9]

The adsorption energy, E_{ads}, of an H_2PO_4 cluster adsorbed on the surface was defined as $E_{ads} = E_{surface} + E_{cluster} - E_{total}$, where $E_{surface}$ is the energy of the bare and relaxed surface, $E_{cluster}$ is the energy of the optimized cluster in a supercell with the same size as the bare surface, and E_{total} is the total energy of the graphene sheet with a cluster, according to the definition, a positive value of E_{ads} corresponds to a thermodynamically favorable adsorption process.

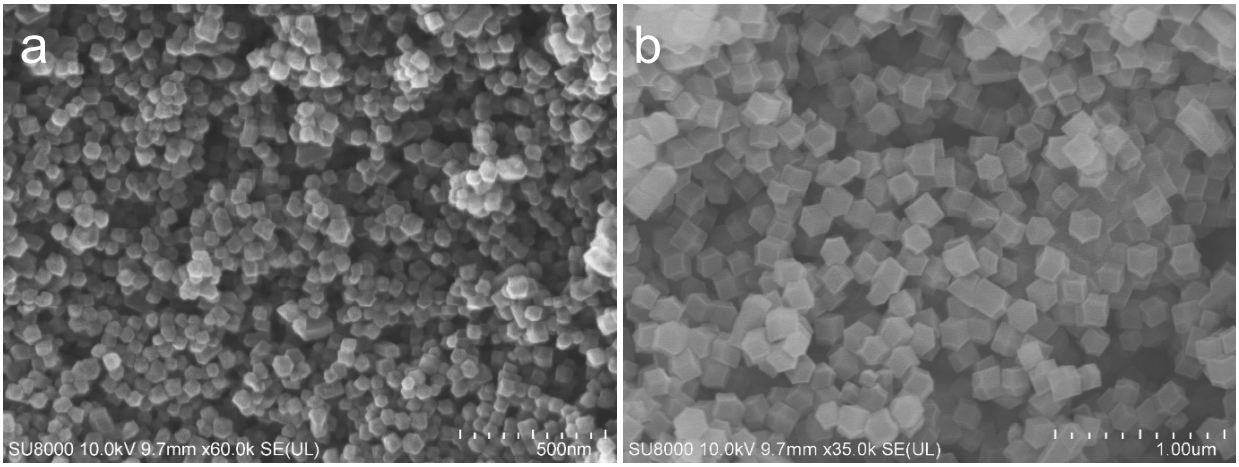

Fig. S1 SEM images of (a) ZIF-8 and (b) Fe-doped ZIF-8.

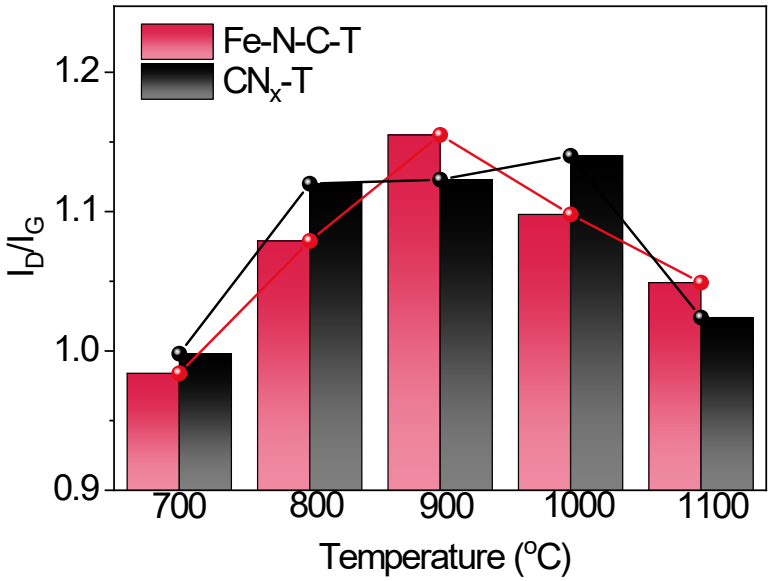

Fig. S2 Comparison of I_D/I_G values of Fe-N-C-T and CN_x-T samples.

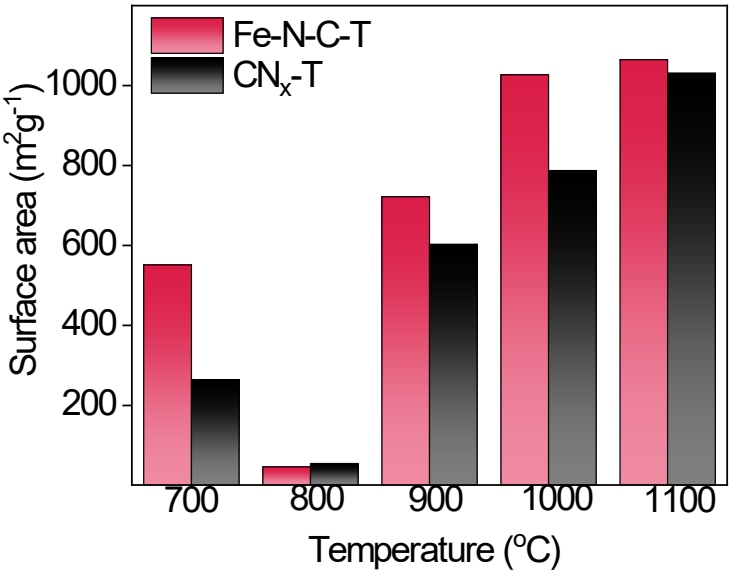

Fig. S3 Surface areas of Fe-N-C-T and CN_x-T samples.

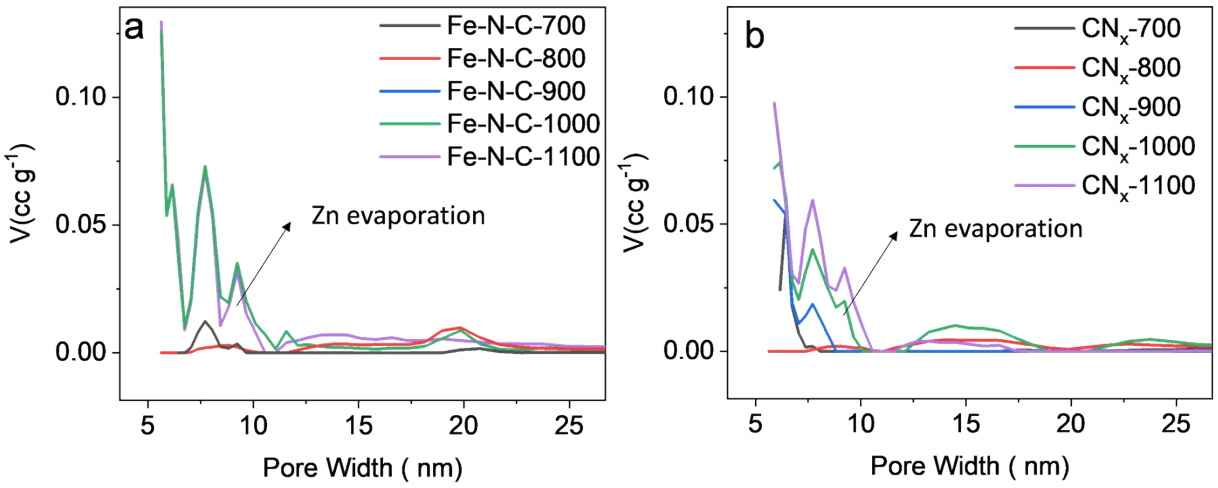

Fig. S4 Pore size distribution of (a) Fe-N-C-T and (b) CN_x-T samples.

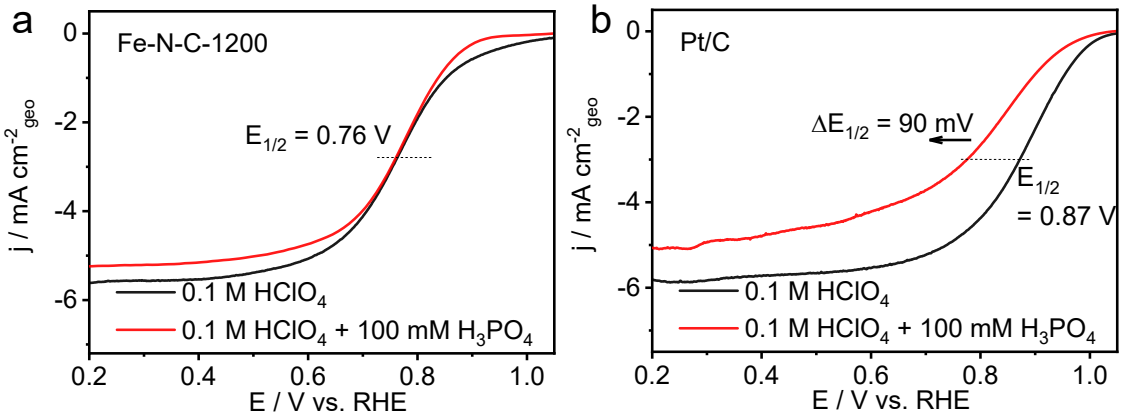

Fig. S5 ORR polarization curves of Fe-N-C-1200 and 20 wt.% Pt/C catalysts in 0.1 M $HClO_4$ (black line) and 0.1 M $HClO_4$ containing 100 mM H_3PO_4 (red line). (Rotaing rate: 1600 rpm; Scan rate: 10 mV s^{-1})

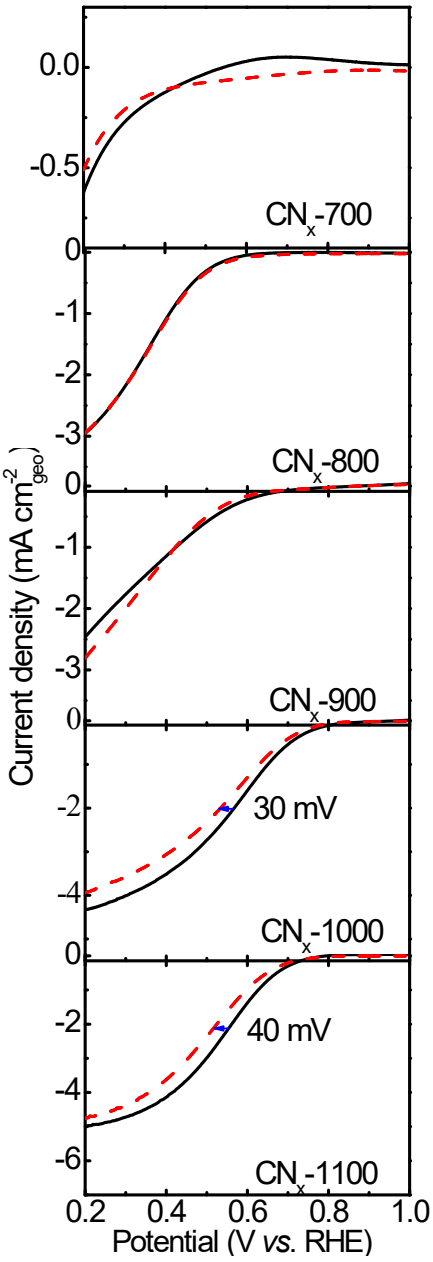

Fig. S6 ORR polarization curves of CN_x-T catalysts in 0.1 M $HClO_4$ (solid lines) and 0.1 M $HClO_4$ containing 100 mM H_3PO_4 (dotted lines).

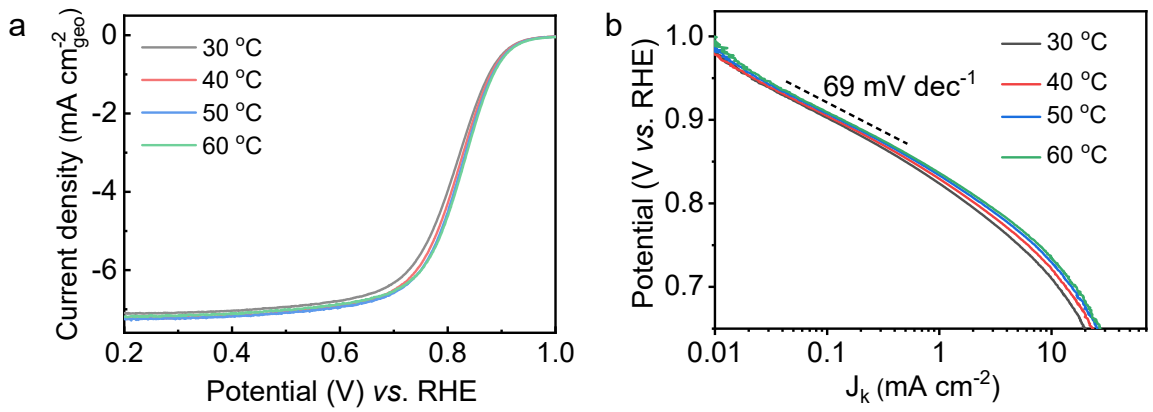

Fig. S7 (a) The ORR polarization curves and the corresponding (b) Tafel plots for Fe-N-C-1100 at different electrolyte temperatures.

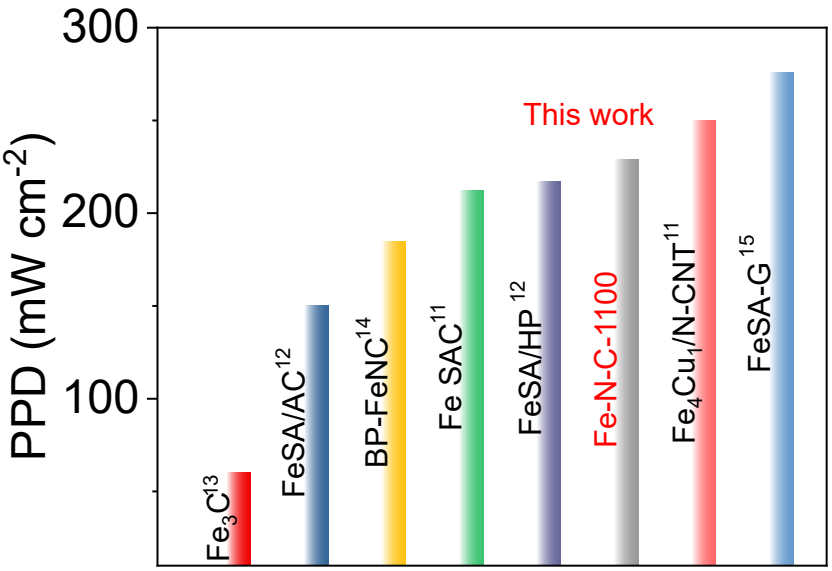

Fig. S8 Comparison of the peak power density (PPD) of the HT-PEMFC with non-precious metal catalysts.

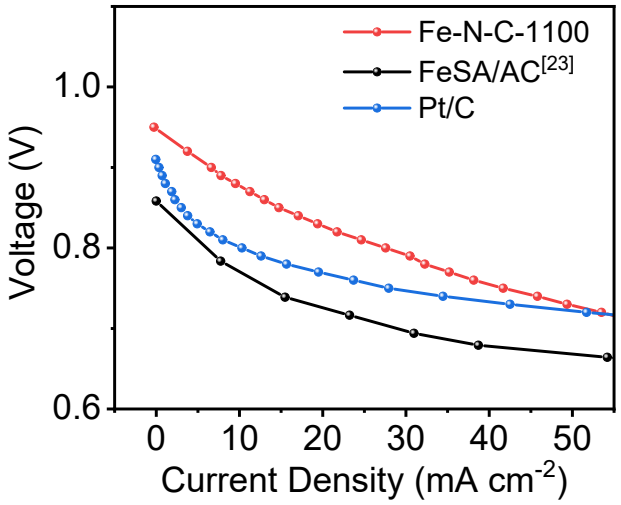

Fig. S9 The enlarged view of the selected region in Fig.3f.

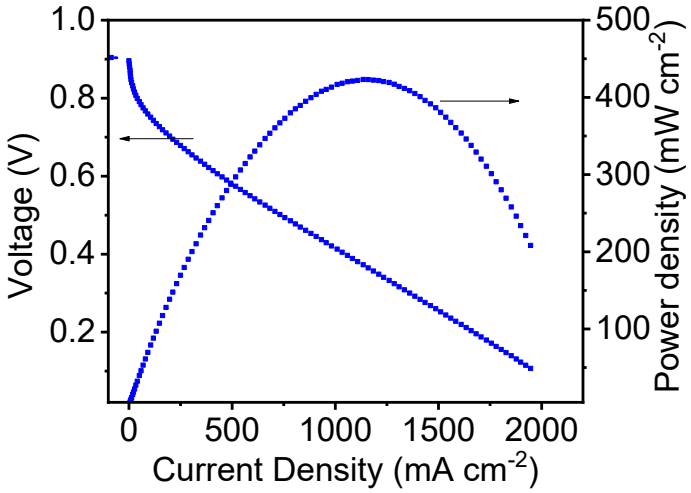

Fig. S10 The discharge curves of PEMFC based on the Fe-N-C-1100 catalyst at 70°C. The anode and cathode were fed full humidified H_2 and O_2 gas at rates of 0.1 L min^{-1} and 0.2 L min^{-1}, respectively, with no backpressure. The cathodic catalyst loading was kept at 3.5 mg cm^{-2}. The Pt loading in the anode was 0.1 mg_{Pt} cm^{-2}.

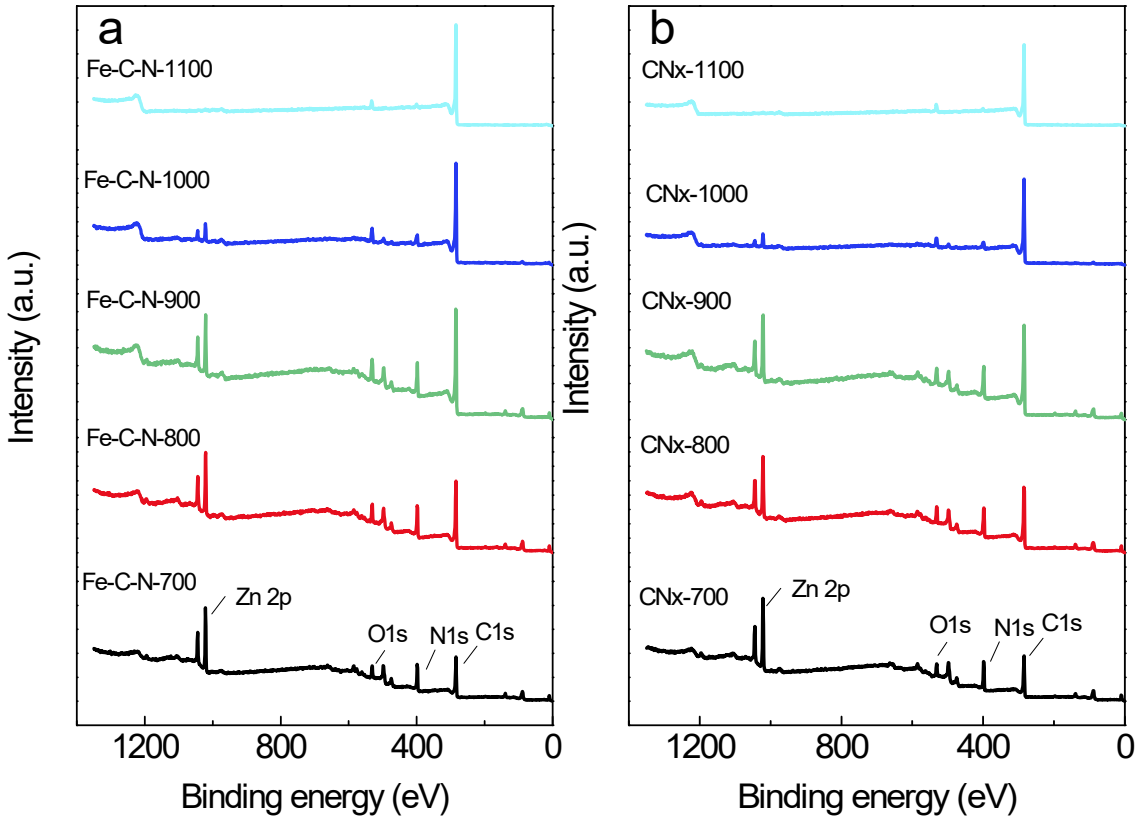

Fig. S11 XPS survey of (a) Fe-N-C-T and (b) CN_x-T. (Note: the other peaks are belong to Zn other orbital peaks.[10])

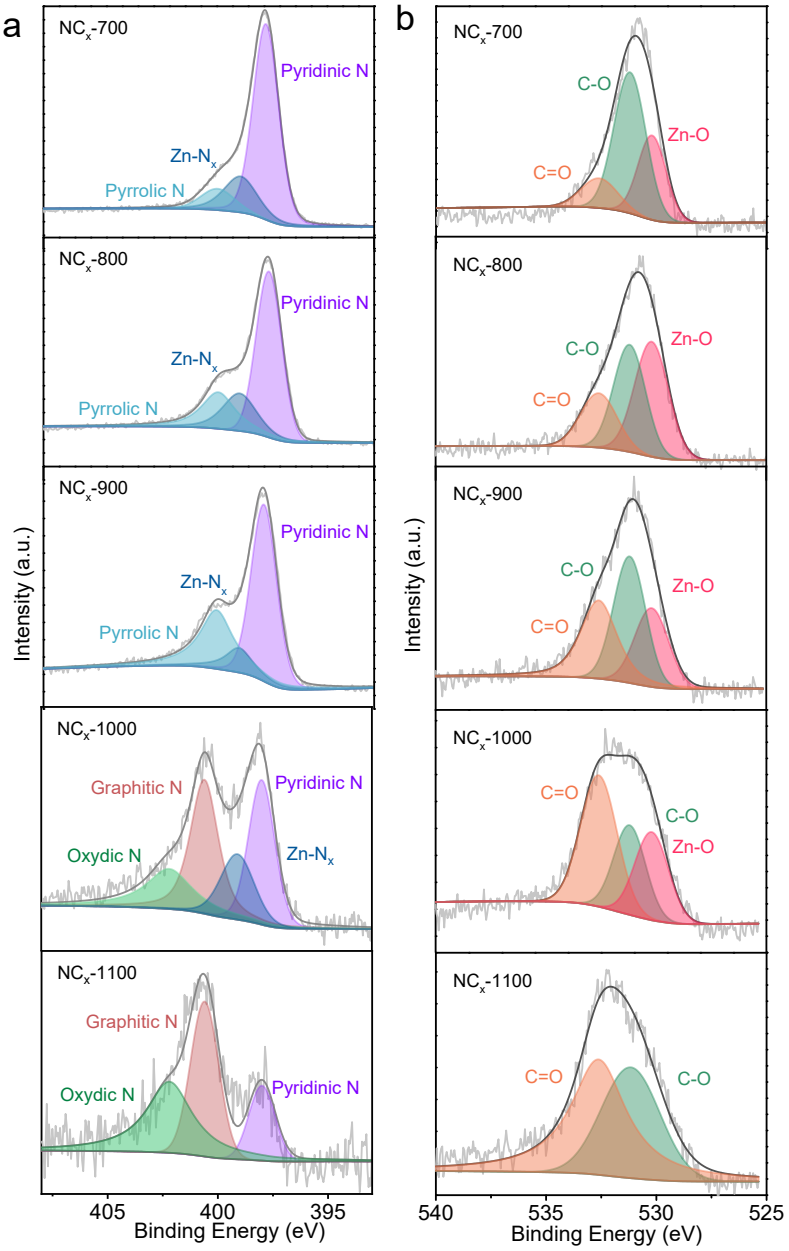

Fig. S12 (a) N 1s XPS spectra and (b) O 1s XPS spectra of CN_x-T samples.

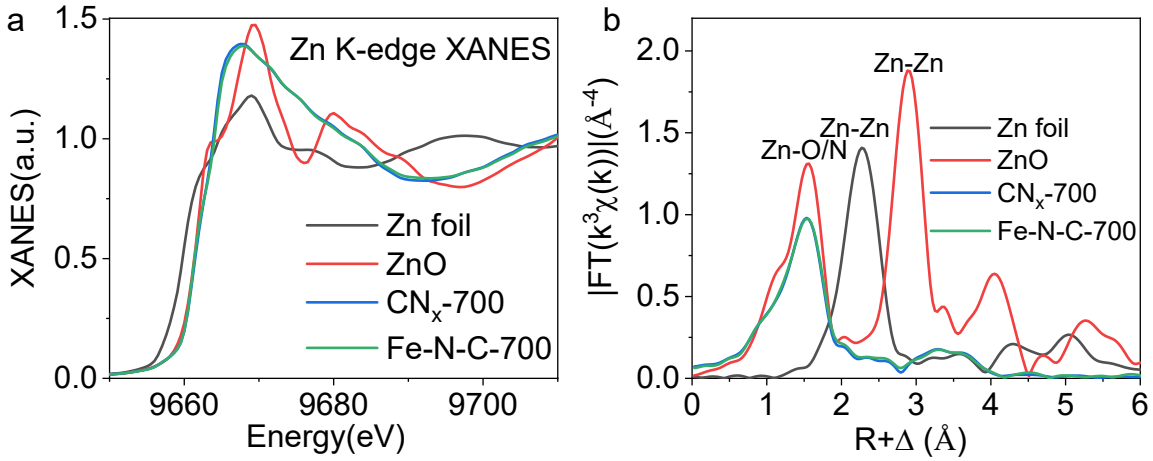

Fig. S13 (a) Zn K-edge XANES spectra and (b) Fourier transforms of k^3-weighted x(k)-function of the EXAFS spectra for Fe-N-C-700 and CN_x-700 samples with Zn foil, ZnO as references.

The Fe-N-C-700 and CN_x-700 Zn K-edge XANES spectra show Zn species in an oxidation state of Zn^{2+}. Furthermore, according to the FT of EXAFS spectra, the peak at 1.53 Å is associated with the scattering of Zn-N/O coordination. There was no Zn-Zn peak detected, indicating that Zn atoms are atomically dispersed.

Table S1. Comparison of peak power density of HT-PEMFC operated with non-precious metal catalysts cathodes.

Cathode catalyst	Anode catalyst	T [°C]	flow rate [anode/ cathode, L min^{-1}]	Peak power density mW cm^{-2}	Ref.
Fe-N-C-1100 3 mg cm^{-2}	**Pt/C 0.3 mg_{Pt} cm^{-2}**	**160**	**0.1/0.2**	**229**	**This work**
Fe_4Cu_1/N-CNTs 4 mg cm^{-2}	Pt/C 1 mg_{Pt} cm^{-2}	230	0.1/0.1	302	11
		160		250	
Fe SAC 4 mg cm^{-2}	Pt/C 1 mg_{Pt} cm^{-2}	230		240	
		160		212	
FeSA/HP 0.6 mg cm^{-2}	Pt/C 1 mg_{Pt} cm^{-2}	240	0.15/0.1	266	12
		160		217	
FeSA/AC 0.6 mg cm^{-2}	Pt/C 1 mg_{Pt} cm^{-2}	160		150	
Fe/C-700(Fe_3C) 6.3 mg cm^{-2}	Pt/C 1.56 mg_{Pt} cm^{-2}	160	-	60	13
BP-FeNC 77.8 mg cm^{-2}	Pt-based electrodes 1.6 mg_{Pt} cm^{-2}	160	0.02/0.02	184.6	14
FeSA-G 0.3 mg_{Fe} cm^{-2}	Pt/C 1 mg_{Pt} cm^{-2}	160	0.1/0.1	276	15
Fe-N-C 2 mg cm^{-2}	Pt/C 1 mg_{Pt} cm^{-2}	160	0.5/0.4	150	16

Table S2. The elemental composition (%) in catalyst surface derived from the XPS spectra in Fig. S11.

Sample	Elemental composition (a.t.%)				
	C	N	O	Fe	Zn
Fe-N-C-700	61.3	22.5	7.3	0.6	8.3
Fe-N-C-800	67.3	18.9	8.1	0.3	5.5
Fe-N-C-900	75.1	13.9	7.1	0.4	3.6
Fe-N-C-1000	84.7	7.7	5.8	0.3	1.5
Fe-N-C-1100	92.7	2.9	4.3	0.2	None
CN_x-700	60.9	23.0	7.4	None	8.7
CN_x-800	68.0	19.0	7.0	None	6.1
CN_x-900	73.5	15.6	6.3	None	4.6
CN_x-1000	87.6	5.9	5.3	None	1.2
CN_x-1100	92.8	2.2	5.0	None	None

Table S3. Deconvolution results of N 1s core level spectra of CN_x-T and Fe-N-C-T.

Catalysts		N 1s Binding Energy (eV)					Relative Intensity (%)	Absolute Intensity (a .t. %)
		Pyridine N	Metal-N_x	Pyrrolic N	Graphitic N	Oxydic N		
CN_x-T	700	397.9	399.1	400.1	-	-	71/18/11/0/0	16.3/4.1/2.5/0/0
	800	397.8	399.1	400.1	-	-	56/21/23/0/0	10.6/4.0/4.4/0/0
	900	398.0	399.1	400.1	-	-	58/13/29/0/0	9.1/2.0/4.5/0/0
	1000	398.0	399.1	-	400.6	402.2	29/17/0/34/20	1.7/1.0/0/2.0/1.2
	1100	398.0	-	-	400.6	402.2	17/0/0/39/44	0.4/0/0/0.9/1.0
Fe- N-C-T	700	398.0	399.1	399.9	-	-	67/18/15/0/0	15.1/4.1/3.4/0/0
	800	398.0	399.1	399.9	-	-	66/17/17/0/0	12.5/3.2/3.2/0/0
	900	397.7	399.0	400.1	-	-	50/21/29/0/0	6.95/2.9/4.0/0/0
	1000	398.0	399.1	-	400.6	402.2	30/23/0/25/22	2.3/1.8/0/1.9/1.7
	1100	398.0	399.1	-	400.6	402.2	14/10/0/40/36	0.4/0.3/0/1.2/1.0

Table S4. Deconvolution results of O 1s core level spectra of CN_x-T and Fe-N-C-T.

Catalysts		O 1s Binding Energy (eV)			Relative Intensity (%)	Absolute Intensity (a. t. %)
		Metal-O	C-O	C=O		
CN_x-T	700	530.2	531.2	532.6	30/56/14	2.2/4.1/1.0
	800	530.2	531.2	532.6	42/37/21	2.9/2.6/1.5
	900	530.2	531.2	532.6	26/39/35	1.6/2.5/2.2
	1000	530.2	531.2	532.6	28/27/45	1.5/1.4/2.4
	1100	-	531.2	532.6	0/40/60	0/2/3
Fe-N-C-T	700	530.2	531.2	532.6	31/54/15	2.3/3.9/1.1
	800	530.2	531.2	532.6	42/36/22	3.4/2.9/1.8
	900	530.2	531.2	532.6	36/30/34	2.6/2.1/2.4
	1000	530.2	531.2	532.6	39/26/35	2.1/1.4/1.9
	1100	530.2	531.2	532.6	18/23/59	0.77/0.99/2.5

Table S5. Summary of fitting parameters of Fe-K-edge EXAFS spectra of Fe-N-C-700 and Fe-N-C-1100 catalysts.

Sample	Atomic Scatter	Coordination Number	Bond Length(Å)	Debye-Waller factor ($10^{-3}\times Å^2$)	R factor
Fe-N-C-700	Fe-N	4	2.01	6.4	0.015
Fe-N-C-1100	Fe-N	5	2.00	8.0	0.010

Table S6. Summary of Bader charges on the atoms of N and C neighbored to Fe in Fe-N_4, Fe-N_5 and Fe-N_4-O.

Atoms	N_4	Fe-N_4	Fe-N_5	Fe-N_4-O
N1	-1.140	-1.138	-1.100	-1.118
N2	-1.177	-1.262	-1.205	-1.080
N3	-1.184	-1.206	-1.150	-1.155
N4	-1.158	-1.2554	-1.221	-1.118
C16	0.554	0.387	0.397	0.408
C18	0.464	0.414	0.631	0.502
C19	0.830	0.405	0.204	0.206
C21	0.640	0.3114	0.531	0.537
C24	0.582	0.313	0.311	0.325
C26	0.623	0.450	0.450	0.459
C27	0.701	0.481	0.4912	0.390
C29	0.405	0.335	0.361	0.371

References

1. Ravel, B.; Newville, M., ATHENA, ARTEMIS, HEPHAESTUS: data analysis for X-ray absorption spectroscopy using IFEFFIT. *J. Synchrotron. Radiat.* **2005,** *12*, 537-541.
2. Kresse, G.; Furthmüller, J., Efficiency of ab-initio total energy calculations for metals and semiconductors using a plane-wave basis set. *Comp. Mater. Sci.* **1996,** *6*, 15-50.
3. G, K.; J, F., Efficient iterative schemes for ab initio total-energy calculations using a plane-wave basis set. *Phys. Rev. B* **1996,** *54*, 11169-11186.
4. Blochl, P. E., Projector augmented-wave method. *Phys. Rev. B* **1994,** 50, 17953-17979.
5. Burke, K.; Ernzerhof, M., Generalized Gradient Approximation Made Simple. *Phys. Rev. Lett.* **1996,** *77*, 3865-3868.
6. Dudarev, S.; Botton, G. A.; Savrasov, S. Y.; Humphreys, C.; Sutton, A. P., Electron-energy-loss spectra and the structural stability of nickel oxide: An LSDA+U study. *Phys. Rev. B* **1998,** *57*, 1505-1509.
7. Liao, P. L.; Carter, E. A., Testing variations of the GW approximation on strongly correlated transition metal oxides: hematite (alpha-Fe_2O_3) as a benchmark. *Phys. Chem. Chem. Phys.* **2011,** *13*, 15189-15199.
8. Grimme, S., Semiempirical GGA-Type Density Functional Constructed with a Long-Range Dispersion Correction. *J. Comput. Chem.* **2006,** *27*, 1787-1799.
9. Bučko, T.; Hafner, J.; Lebègue, S.; Ángyán, J. G., Improved Description of the Structure of Molecular and Layered Crystals: Ab Initio DFT Calculations with van der Waals Corrections. *J. Phys. Chem. A* **2010,** *114*, 11814-11824
10. Kaneti, Y. V.; Zhang, Z.; Yue, J.; Zakaria, Q. M. D.; Chen, C.; Jiang, X.; Yu, A., Crystal plane-dependent gas-sensing properties of zinc oxide nanostructures: experimental and theoretical studies. *Phys. Chem. Chem. Phys.* **2014,** *16*, 11471-11480.
11. Cheng, Y.; Wang, M.; Lu, S.; Tang, C.; Wu, X.; Veder, J.-P.; Johannessen, B.; Thomsen, L.; Zhang, J.; Yang, S.-z.; Wang, S.; Jiang, S. P., First demonstration of phosphate enhanced atomically dispersed bimetallic FeCu catalysts as Pt-free cathodes for high temperature phosphoric acid doped polybenzimidazole fuel cells. *Appl. Catal. B: Environ.* **2021,** *284*, 119717.
12. Cheng, Y.; Zhang, J.; Wu, X.; Tang, C.; Yang, S.-z.; Su, P.; Thomsen, L.; Zhao, F.; Lu, S.; Liu, J.; Jiang, S. P., A template-free method to synthesis high density iron single atoms anchored on carbon nanotubes for high temperature polymer electrolyte membrane fuel cells. *Nano Energy* **2021,** *80*, 105534.
13. Hu, Y.; Jensen, J. O.; Zhang, W.; Martin, S.; Chenitz, R.; Pan, C.; Xing, W.; Bjerrum, N. J.; Li, Q., Fe3C-based oxygen reduction catalysts: synthesis, hollow spherical structures and applications in fuel cells. *J. Mater.Chem. A* **2015,** *3*, 1752-1760.
14. Hu, Y.; Jensen, J. O.; Pan, C.; Cleemann, L. N.; Shypunov, I.; Li, Q. F., Immunity of the Fe-N-C catalysts to electrolyte adsorption: Phosphate but not perchloric anions. *Appl. Catal. B-Environ.* **2018,** *234*, 357-364.
15. Cheng, Y.; He, S.; Lu, S.; Veder, J.-P.; Johannessen, B.; Thomsen, L.; Saunders, M.; Becker, T.; De Marco, R.; Li, Q.; Yang, S.-z.; Jiang, S. P., Iron single atoms on graphene as nonprecious metal catalysts for high-temperature polymer electrolyte membrane fuel cells. *Adv. Sci.* **2019,** *6*, 1802066.
16. Gokhale, R.; Asset, T.; Qian, G.; Serov, A.; Artyushkova, K.; Benicewicz, B. C.; Atanassov, P., Implementing PGM-free electrocatalysts in high-temperature polymer electrolyte membrane fuel cells. *Electrochem. Commun.* **2018,** *93*, 91-94.